Modeling Atrial Fiber Orientation in Patient-Specific Geometries: A Semi-automatic Rule-Based Approach

Martin W. Krueger[1], Viktor Schmidt[1], Catalina Tobón[2], Frank M. Weber[1], Cristian Lorenz[3], David U.J. Keller[1], Hans Barschdorf[3], Michael Burdumy[1], Peter Neher[1,3], Gernot Plank[4], Kawal Rhode[5], Gunnar Seemann[1], Damien Sanchez-Quintana[6], Javier Saiz[2], Reza Razavi[5], and Olaf Dössel[1]

[1] Institute of Biomedical Engineering, Karlsruhe Institute of Technology (KIT), Germany
martin.krueger@kit.edu
http://www.ibt.kit.edu
[2] Grupo Bioelectrónica- I3BH, Universidad Politécnica de Valencia, Spain
[3] Philips Research Hamburg, Germany
[4] Institute of Biophysics, Medical University of Graz, Austria
[5] Division of Imaging Sciences and Biomedical Engineering, King's College London, United Kingdom
[6] Department of Anatomy, Universidad de Extramadura, Badajoz, Spain

Abstract. Atrial myofiber orientation is complex and has multiple discrete layers and bundles. A novel robust semi-automatic method to incorporate atrial anisotropy and heterogeneities into patient-specific models is introduced. The user needs to provide 22 distinct seed-points from which a network of auxiliary lines is constructed. These are used to define fiber orientation and myocardial bundles. The method was applied to 14 patient-specific volumetric models derived from CT, MRI and photographic data. Initial electrophysiological simulations show a significant influence of anisotropy and heterogeneity on the excitation pattern and P-wave duration (20.7 % shortening). Fiber modeling results show good overall correspondence with anatomical data. Minor modeling errors are observed if more than four pulmonary veins exist in the model. The method is an important step towards creating realistic patient-specific atrial models for clinical applications.

Keywords: patient-specific modeling, atrial modeling, fiber orientation, atrial heterogeneity, atrial anisotropy.

1 Introduction

Atrial anisotropy has strong influence on excitation propagation, activation pattern and P-wave duration (PWd). Simulated P-waves from isotropic models show longer PWds compared to measurements. The use of atrial models in clinical practice therefore requires realistic patient-specific conduction properties.

D.N. Metaxas and L. Axel (Eds.): FIMH 2011, LNCS 6666, pp. 223–232, 2011.

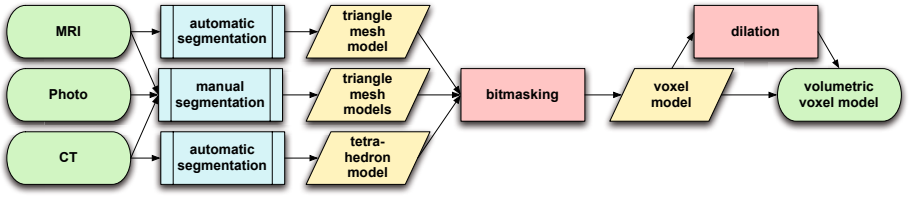

Fig. 1. Workflow to generate volumetric voxel models from various data entities

Atrial myocardial fibers also play an important role in the development and perpetuation of atrial arrhythmias [1].

Incorporating myocardial fiber orientation in atrial models has been going on for nearly a decade now [2,3]. So far, only singular anatomies were manually enhanced with fiber orientation [1,2,3,4,5,6]. Due to most models being 3D surface models [2,3,4,5] they cannot reproduce complex, multi-layer atrial anisotropy. Available volumetric models show only transmurally constant myofiber orientation [1,6], neglecting intersecting fiber bundles. In contrast, ventricular myofiber information is commonly placed automatically in patient-specific models using rule-based or statistical [7] approaches. Recently semi-automatic approaches to add sparse anisotropy in atrial models were reported [8,9,10].

We present a robust semi-automatic method to incorporate complete multi-layer myocardial fiber orientation in patient-specific 3D volumetric models of the human atria. Myocardial tissue is classified to incorporate known atrial heterogeneities [11]. Knowledge about atrial myofiber orientation was gained from literature [12,13,14] as well as from photographic data of human atrial preparations.

2 Methods

2.1 Patient-Specific Atrial Models

Patient-specific isotropic atrial models were created from six volunteers and six patients. The model generation workflow is shown schematically in Figure 1. From the image data, surface models were generated. MRI datasets (n=8) were segmented using automatic (n=5) [15] and manual (n=3) approaches. CT datasets (n=4) were segmented using an automatic method [16]. Photographic data (n=2, Visible Human Man, Visible Human Female) were segmented manually. Volumetric voxel models were created from the surface models. Data segmented with a method described in [15] lack epicardial surface meshes. The endocardium was therefore dilated to produce a model with a homogeneous wall thickness of 2.5-3 mm [17], which corresponds to 7-10 voxels transmurally at a resolution of 0.33 mm.

2.2 Tissue Classification and Fiber Generation

Tissue classification and fiber generation can be separated into multiple sequential steps (Fig. 2). The method uses a volumetric atrial voxel model as input and

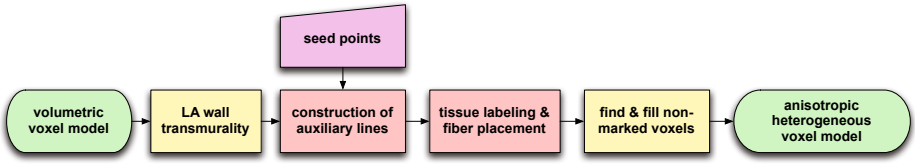

Fig. 2. Workflow of the presented method. Green: input / output; yellow: pre- and post-processing steps; red: algorithm steps; pink: user input.

enhances this with anisotropy and heterogeneity information. In a preparation step, the left atrial wall is split into two equidistant layers through the computation of a virtual static electric field. The steady state "potential distribution" between blood pool and epicardium is thereby calculated by solving Poisson's equation and the left atrial wall is separated at mid potential.

The algorithm requires the user to provide coordinates of 22 seed points in the right and left atrium (Fig. 3 blue points). From the seed points, auxiliary lines and further landmarks (intersection of auxiliary lines) were calculated (Fig. 3 dashed lines) using an adapted 3D fast marching level set method [18] to determine the shortest paths between different coordinates (Fig. 4a). For some myocardial structures (e. g. Crista Terminalis, points R3-R4 in Fig. 3) the shortest path method did not provide the best possible results. In these cases, a corridor along specific planes derived from three seed or auxiliary points was created as boundary condition of the fast marching algorithm. For all seed points used to generate circular muscle bundles (e. g. R1-3, R7-9, L1-3 in Fig. 3) we noted that the points needed to be about equally spaced around the rim, as the shortest paths between the points were used to generate the circular structure of the muscle.

Some of the constructed paths (Fig. 3, solid lines) were used as borders for atrial regions (Fig. 4, bottom row) or as center line for myocardial bundles (Fig. 4, top row). The voxels belonging to these paths were labeled for the corresponding tissue type and the fiber orientation was set along the paths (Fig. 4a,b). Constructed fibers were spatially linear low pass filtered afterwards (Fig. 4c). Thereby, the orientations of the five preceding and five succeeding fiber vectors were averaged. This effectively smoothened abrupt changes in fiber direction and discretization artifacts.

The voxels enclosed by the paths were marked using a 3D implementation of the region growing method [19] to classify their tissue properties (Fig. 4d). If a path marked a muscle bundle (e. g. Crista Terminalis, interatrial bundles, ring muscles), the center line was dilated to produce transverse extension. Fiber orientations within the region were calculated from the average of distance-weighted border voxel orientations (Fig. 4e). In a post-processing step (Fig. 2, yellow) all non-classified voxels were appended to the closest region. Fiber orientation in these voxels was calculated from the average of the surrounding border orientations. Output of this procedure was a volumetric anisotropic heterogeneous bi-atrial voxel model with bundles and regions having smoothly varying fiber

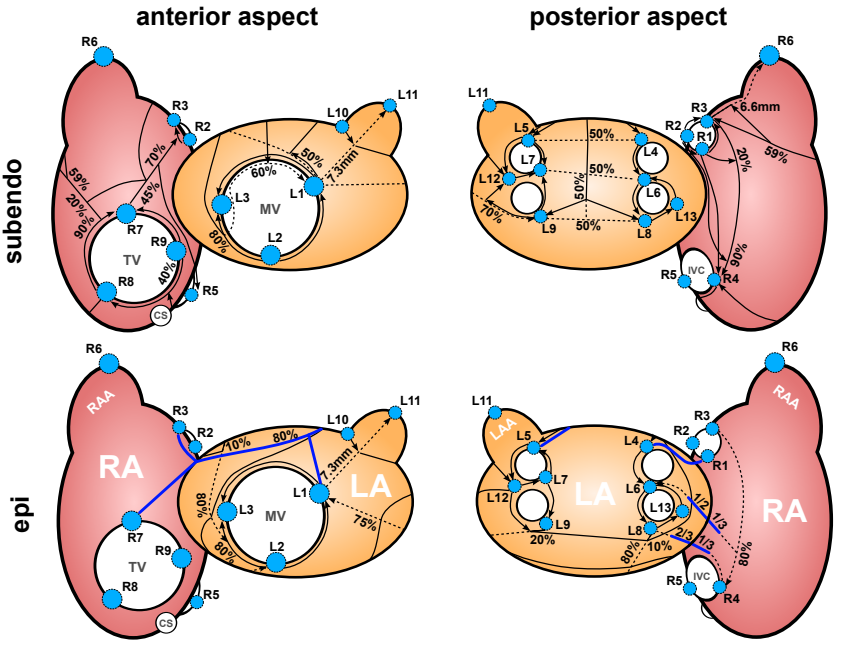

Fig. 3. Seed points (light blue), auxiliary lines (dashed) and region borders (solid lines). Interatrial connections are shown in blue. Arrows indicate the directions of fast marching shortest paths. RA(A): right atrium (appendage); LA(A): left atrium (appendage); TV: tricuspid valve; MV: mitral valve; CS: coronary sinus; IVC: inferior caval vein.

orientation within them, but can cross each other in different transmural layers in a discontinuous manner.

2.3 Electrophysiological Simulations

Two simulations were performed with one model (volunteer, MRI, automatic segmentation, Δx=0.33 mm) to investigate the impact of the anisotropy on atrial excitation. The Courtemanche-Ramirez-Nattel (CRN) model of human atrial electrophysiology [20] was used to simulate atrial action potentials. Maximum ion conductances for three potassium currents were adjusted such that the CRN model was able to reproduce action potentials from various atrial tissues [6]. Cell coupling was considered by the monodomain equation. Finite elements and the explicit Euler method with a time increment of 20 μs were used to discretize the equations in a C++ simulation framework [21]. Transversal conductivity was set to 0.075 S/m for regular atrial myocardium, appendages, valve rings and the right atrial isthmus, to 0.181 S/m for Bachmann's Bundle, 0.075 S/m for Crista Terminalis, 0.03 S/m for pectinate muscles and 0.275 S/m for the sinus node. Ratios for transverse to longitudinal conductivity were to set to 3.75 for regular atrial myocardium and appendages, 3.63 for valve rings, 1.0 for isthmus

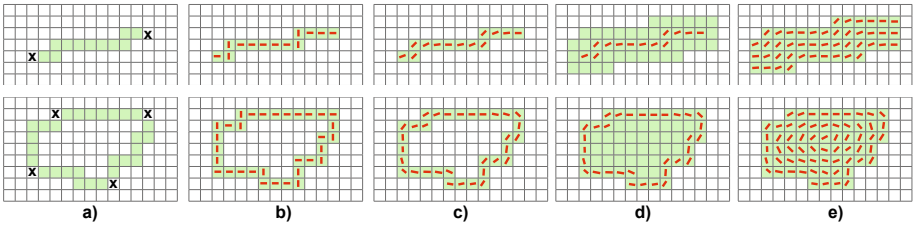

Fig. 4. Region classification and fiber placement in bundles (upper row) and regions (lower row) exemplary shown in a 2D grid. Methods are implemented in 3D and work analogue to the shown examples. a) Shortest path between seed and/or auxiliary points mark region borders. b) Fiber orientation is set along borders. c) Fiber orientation smoothened by averaging of pre- and succeeding orientations. d) Inner region marked using region growing. e) Fiber orientation calculated from the average of distance-weighted border orientations.

and the sinus node, 3.88 for Bachmann's Bundle, 6.56 for Crista Terminalis and 23.25 for pectinate muscles to produce conduction velocities comparable to [22]. Atrial activation was initiated at the location of the sinus node with a basic cycle length of 800 ms. Prior to the coupled cell simulation, 50 cycles of isolated cell simulations were run to reach steady state conditions.

3 Results

3.1 Fiber Orientation and Tissue Classification

We applied the presented method to 14 patient-specific atrial models derived from CT, MR and photographic data. Global fiber orientation in the atrial models showed circulating muscle bundles around the valve openings (Fig. 5d), around the orifice of the superior caval vein and around the pulmonary vein orifices. Atrial appendages had circular fibers, showing some discretization error at their tip. Right atrial appendage fibers arose from the septum spurium and the tricuspid valve musculature (Fig. 5a). Septo-atrial and septo-pulmonary bundles were overlaying each other in the LA roof (Fig. 5c). Bachmann's Bundle, Crista Terminalis and pectinate muscles had well aligned fibers along their longitudinal extent. Fifteen pectinate muscles arose perpendicular from Crista Terminalis in the right atrium and end at the tricuspid ring in the same manner (Fig. 5a,c). Crista Terminalis was crossed by fibers of the intercaval bundles in the subepicardium, which were merging with the pectinate muscles fibers afterwards (Fig. 5a). The area between the intercaval bundle and the orifice of the inferior caval vein was isotropic.

3.2 Influence of Atrial Anisotropy on Excitation Sequence

Two simulations on one geometry were performed: one using the homogeneous isotropic case and one with added electrophysiological heterogeneities and anisotropy. Activation was initiated at the site of the sinus node in both cases

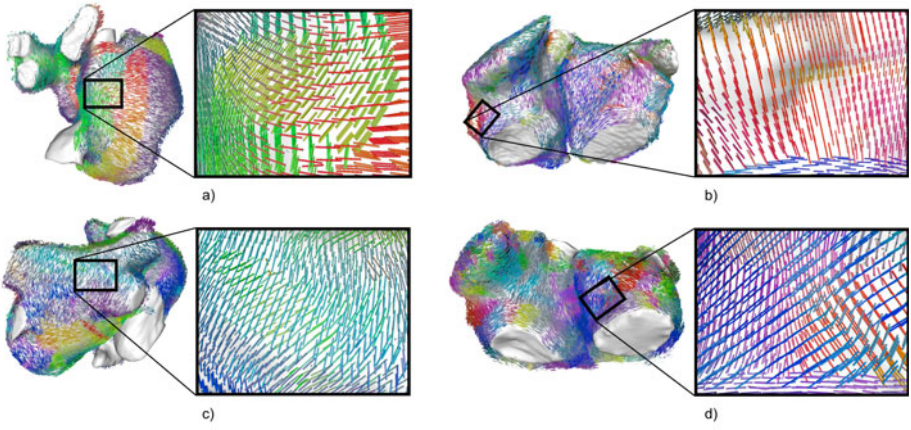

Fig. 5. Examples of generated fibers in different models. Local fiber direction is shown by color-coded cylinders. Inlays show close up transmural fiber structure. a) Fibers from intercaval bundle cross Crista Terminalis epicardially. b) Septo-atrial and septo-pulmonary bundles arise from the mitral valve ring muscle. c) Two layers of myofibers in the left atrial roof. d) Pectinate muscle fibers connecting perpendicular to the tricuspid valve ring musculature.

(Fig. 6, 20 ms). In the isotropic case, excitation spread circular in contrast to the enhanced model, where activation spread over fast conducting Crista Terminal and pectinate muscles (32 ms). The left atrium was activated from the anterior side via Bachmann's Bundle in the enhanced case, whereas slower left atrial activation in the homogeneous model arose from the right superior pulmonary vein (47 ms). Myofibers circulating the pulmonary veins influenced the excitation wavefront (47 ms). Heterogeneous electrophysiological properties of the Crista Terminalis influenced right atrial electrophysiology in the enhanced model (78 ms). Complete atrial activation was achieved after 145 ms in the isotropic case and after 115 ms in the enhanced model (-30 ms / -20.7%). The duration of the corresponding simulated P-waves was reduced from 145 ms to 115 ms (not shown). Measured PWd of the same subject was ca. 100 ms.

4 Discussion and Conclusion

We presented a novel approach to incorporate complete anisotropy into patient-specific human atrial models. The proposed method worked reliably in 14 datasets (MRI, CT, photographic data). Information on atrial fiber architecture is very sparse. 3D information on atrial fibers (e. g. DT-MRI) is not available, as atria in these datasets are collapsed and show strong artifacts at tissue borders. Due to the thin atrial wall, fibers cannot be extracted from high resolution photographic data as done for the ventricles [23], except from large muscular bundles as Crista Terminalis, Bachmann's Bundle and pectinate muscles [6]. In future it might be possible to image ventricular fiber structure in-vivo using DT-MRI [24]. Nevertheless, the problems caused by the thin atrial wall will persist

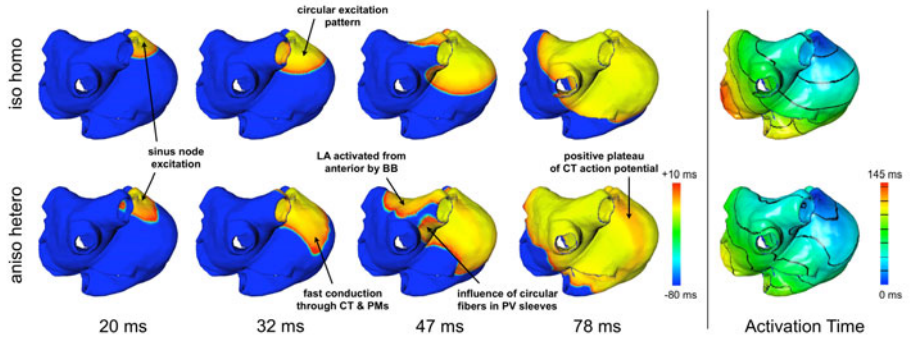

Fig. 6. Simulation of atrial electrophysiology in an isotropic homogeneous model (top row) and in the corresponding anisotropic heterogeneous model (bottom row). Shown are the transmembrane voltage distributions at four time instances as well as the activation time maps (right).

and thus, such in-vivo methods will not be available to image atrial fibers for a long time. On the other hand, as MRI resolution advances, it could be possible to image atrial fibers of excised human atria using DT-MRI ex-vivo, if suitable preparation techniques are used.

Atrial myocardial structure is known to show inter-individual differences. We concentrated on modeling the most common myofiber structure described in literature. Myofibers in the appendages can show systematic or chaotic patterns [14]. As this information cannot be extracted from patient-specific data, we chose to model circular fibers to gain reproducible results. We included three posterior interatrial muscle bundles and Bachmann's Bundle anterior as the major right to left atrial pathway. The posterior connections were found in 67% - 93% of excised hearts and Bachmann's Bundle is absent only in few people [14]. As all our models lacked the coronary sinus, we neglected interatrial connections arising from this musculature.

Others have shown high resolution anisotropic models of parts of animal atria [25,26] with very complex fiber structure. We aim at providing anisotropy for human bi-atrial models. Due to the resulting limited spatial resolution, we introduced some simplifications of myofiber structure. We observed sites of chaotic fiber intersection in models which have more than four pulmonary veins or early branching of those. The algorithm was developed for atrial geometries with four pulmonary veins, which covers about two thirds of all human atria [27]. If sufficient information on fiber structure around uncommon pulmonary vein configurations is available, we will adapt our method accordingly. Various pathologies are known to influence global and local fiber architecture, e. g. structural remodeling or fibrosis in atrial fibrillation patients. The method could in future be adapted to reflect such pathologies.

The semi-automatic approach requires user input for 22 seed points. This bears potential for individual variations in seed point placement, which we adjusted the algorithm to cope with. The method could be coupled to automatic

segmentation techniques [15,16] by marking seed points in the statistical model, thus removing user based variations. Analyzing the sensitivity of the algorithm to user introduced variations of the seed points is strongly implementation-dependent and would outrun the scope the this study. The prospect to couple the presented method with automatic segmentation algorithms will make such analysis obsolete.

Evaluation and validation of fiber modeling is a crucial point for the reliability of the model. We compared the modeling results with data from literature [12,13,14] and unpublished photographs. In all cases, modeled fiber direction showed good correspondence with the data. Application of the algorithm to animal data with known fiber orientation [25,26] for validation is difficult, as atrial fiber architecture is not unconditionally comparable between animal and human. Simulated anisotropic activation time maps are in agreement with measured activation time patterns in human [28,29,30]. Measurements showed that activation in the right atrium is faster along Crista Terminalis [29,30] and that the left atrium is activated by two wavefronts from anterior and right-posterior to activate the region left-inferior of the left inferior pulmonary vein at latest during sinus rhythm [28,29]. These effects were also observed in all our anisotropic simulations.

The simulation results highlight the impact of anisotropy in patient-specific atrial models on atrial activation pattern and PWd. Shortening of simulated P-wave caused by electrophysiological heterogeneities and anisotropy resulted in a better correspondence to measured PWd of the same subject. PWd could also be matched by adjustment of global conduction velocity in isotropic models. Doing so would result in conduction velocities greater than those measured in healthy human [31]. This indicates that the modeling error in homogeneous models is greater than in models with rule-based fibers and heterogeneities. Although the presented method is focused on modeling global fiber architecture, further evaluation of the sensitivity of the excitation sequence to small changes in fiber structure will be necessary. Comprehensive studies with more models will need to further address these topics. The presented method is an important step to introduce reliable patient-specific atrial models into clinical practice.

Acknowledgments. The authors would like to thank Bettina Schwab and Wilfried Dzeakou for their contribution to the segmentation of the MRI data. Furthermore the authors would like to thank Alexandra Groth, Philips Research Hamburg, for the support regarding the automatic segmentation.

The research leading to these results has received funding from the European Communitys Seventh Framework Programme (FP7/2007-2013) under grant agreement no 224495 (euHeart project).

References

1. Plank, G., Prassl, A.J., Wang, J.I., Seemann, G., Scherr, D., Sanchez-Quintana, D., Calkins, H., Trayanova, N.A.: Atrial fibrosis promotes the transistion of pulmonary vein ectopy into reentrant arrhathmias. In: Heart Rhythm (2008)

2. Vigmond, E.J., Ruckdeschel, R., Trayanova, N.: Reentry in a morphologically realistic atrial model. Cardiovasc Electrophysiol. 12, 1046–1054 (2001)
3. Zemlin, C., Herzel, H., Ho, S., Panfilov, A.: A realistic and efficient model of excitation propagation in the human atria. In: Computer Simulation and Experimental Assessment of Cardiac Electrophysiology, Futura, pp. 29–34 (2001)
4. Jacquemet, V.: A biophysical model of atrial fibrillation and electrograms: formulation, validation and applications. PhD thesis (2004)
5. Tobón, C., Ruiz, C., Heidenreich, E., Hornero, F., Sáiz, J.: Effect of the ectopic beats location on vulnerability to reentries in a three-dimensional realistic model of human atria. Computers in Cardiology 36, 449–452 (2009)
6. Seemann, G., Höper, C., Sachse, F.B., Dössel, O., Holden, A.V., Zhang, H.: Heterogeneous three-dimensional anatomical and electrophysiological model of human atria. Phil. Trans. Roy. Soc. A 364, 1465–1481 (2006)
7. Peyrat, J.-M., Sermesant, M., Pennec, X., Delingette, H., Xu, C., McVeigh, E.R., Ayache, N.: A computational framework for the statistical analysis of cardiac diffusion tensors: application to a small database of canine hearts. IEEE Transactions on Medical Imaging 26, 1500–1514 (2007)
8. Hermosillo, B.D.F.: Semi-automatic enhancement of atrial models to include atrial architecture and patient specific data: For biophysical simulations. Computers in Cardiology 35, 633–636 (2008)
9. Krueger, M.W., Weber, F.M., Seemann, G., Dössel, O.: Semi-automatic segmentation of sinus node, bachmann's bundle and terminal crest for patient specific atrial models. In: World Congress on Medical Physics and Biomedical Engineering. IFMBE Proceedings, vol. 25/4, pp. 673–676. Springer, Heidelberg (2009)
10. Krueger, M.W., Rhode, K., Weber, F.M., Keller, D.U.J., Caulfield, D., Seemann, G., Knowles, B.R., Razavi, R., Dössel, O.: Patient-specific volumetric atrial models with electrophysiological components: A comparison of simulations and measurements. Biomedizinische Technik / Biomedical Engineering 55(s1), 54–57 (2010)
11. Feng, J., Yue, L., Wang, Z., Nattel, S.: Ionic mechanisms of regional action potential heterogeneity in the canine right atrium. Circ. Res. 83, 541–551 (1998)
12. Papez, J.W.: Heart musculature of the atria. Am. J. Anatomy 27, 255–286 (1920)
13. Sanchez-Quintana, D., Anderson, R., Cabrera, J., Climent, V., Martin, R., Farre, J., Ho, S.: The terminal crest: morphological features relevant to electrophysiology. Heart (British Cardiac Society) 88, 406–411 (2002)
14. Ho, S., Sanchez-Quintana, D.: The importance of atrial structure and fibers. Clinical Anatomy (New York, N.Y.) 22, 52–63 (2009)
15. Ecabert, O., Peters, J., Schramm, H., Lorenz, C., von Berg, J., Walker, M., Vembar, M., Olszewski, M., Subramanyan, K., Lavi, G., Weese, J.: Automatic model-based segmentation of the heart in ct images. IEEE Transactions on Medical Imaging 27, 1189–1201 (2008)
16. Weese, J., Peters, J., Meyer, C., Wächter, I., Kneser, R., Lehmann, H., Ecabert, O., Barschdorf, H., Hanna, R., Weber, F.M., Dössel, O., Lorenz, C.: The generation of patient-specific heart models for diagnosis and interventions. In: Camara, O., Pop, M., Rhode, K., Sermesant, M., Smith, N., Young, A. (eds.) STACOM 2010. LNCS, vol. 6364, pp. 25–35. Springer, Heidelberg (2010)
17. Platonov, P.G., Ivanov, V., Ho, S.Y., Mitrofanova, L.: Left atrial posterior wall thickness in patients with and without atrial fibrillation: data from 298 consecutive autopsies. Cardiovasc Electrophysiol. 19, 689–692 (2008)
18. Baerentzen, J.: On the implementation of fast marching methods for 3D lattices. Technical report (2001)

19. Wan, S.Y., Higgins, W.E.: Symmetric region growing. IEEE Transactions on Image Processing 12, 1007–1015 (2003)
20. Courtemanche, M., Ramirez, R.J., Nattel, S.: Ionic mechanisms underlying human atrial action potential properties: Insights from a mathematical model. Am. J. Physiol. 275, H301–H321 (1998)
21. Seemann, G., Sachse, F.B., Karl, M., Weiss, D.L., Heuveline, V., Dössel, O.: Framework for modular, flexible and efficient solving the cardiac bidomain equation using petsc. Progr. Industr. Math. 15, 363–369 (2010)
22. Harrild, D.M., Henriquez, C.S.: A computer model of normal conduction in the human atria. Circ. Res. 87, 25 (2000)
23. Sachse, F., Frech, R., Werner, C., Dössel, O.: A model based approach to assignment of myocardial fibre orientation. In: Proceedings of Computers in Cardiology, Hannover, pp. 145–148 (1999)
24. Toussaint, N., Sermesant, M., Stoeck, C.T., Kozerke, S., Batchelor, P.G.: *In vivo* human 3D cardiac fibre architecture: Reconstruction using curvilinear interpolation of diffusion tensor images. In: Jiang, T., Navab, N., Pluim, J.P.W., Viergever, M.A. (eds.) MICCAI 2010. LNCS, vol. 6361, pp. 418–425. Springer, Heidelberg (2010)
25. Zhao, J., Trew, M.L., Legrice, I.J., Smaill, B.H., Pullan, A.J.: A tissue-specific model of reentry in the right atrial appendage. Cardiovasc Electrophysiol. 20, 675–684 (2009)
26. Campos, F.O., Wiener, T., Prassl, A.J., Ahammer, H., Plank, G., Weber Dos Santos, R., Sanchez-Quintana, D., Hofer, E.: A 2D-computer model of atrial tissue based on histographs describes the electro-anatomical impact of microstructure on endocardiac potentials and electric near-fields. In: Annual International Conference of the IEEE EMBC Society, vol. 1, pp. 2541–2544 (2010)
27. Marom, E., Herndon, J., Kim, Y., McAdams, H.: Variations in pulmonary venous drainage to the left atrium: implications for radiofrequency ablation. Radiology 230, 824–829 (2004)
28. Boineau, J.P., Canavan, T.E., Schuessler, R.B., Cain, M.E., Corr, P.B., Cox, J.L.: Demonstration of a widely distributed atrial pacemaker complex in the human heart. Circ. 77, 1221–1237 (1988)
29. De Ponti, R., Ho, S.Y., Salerno-Uriarte, J.A., Tritto, M., Spadacini, G.: Electroanatomic analysis of sinus impulse propagation in normal human atria. Journal of Cardiovascular Electrophysiology 13, 1–10 (2002)
30. Wang, L., Zhang, H., Wong, K.C.L., Liu, H., Shi, P.: Noninvasive imaging of electrophysiological substrates in post myocardial infarction. In: Yang, G.-Z., Hawkes, D., Rueckert, D., Noble, A., Taylor, C. (eds.) MICCAI 2009. LNCS, vol. 5762, pp. 732–740. Springer, Heidelberg (2009)
31. Hansson, A., Holm, M., Blomstrom, P., Johansson, R., Luhrs, C., Brandt, J., Olsson, S.: Right atrial free wall conduction velocity and degree of anisotropy in patients with stable sinus rhythm studied during open heart surgery. Eur. Heart. J. 19, 293–300 (1998)